Changes in background aerosol composition in Finland during polluted and clean periods studied by TEM/EDX individual particle analysis

J. V. Niemi, S. Saarikoski, H. Tervahattu, T. Mäkelä, R. Hillamo, H. Vehkamäki, L. Sogacheva, M. Kulmala

Atmos. Chem. Phys. Discuss., 6, 6753–6799, 2006
www.atmos-chem-phys-discuss.net/6/6753/2006/

Atmospheric Chemistry and Physics Discussions

Changes in background aerosol composition in Finland during polluted and clean periods studied by TEM/EDX individual particle analysis

J. V. Niemi[1], S. Saarikoski[2], H. Tervahattu[3], T. Mäkelä[2], R. Hillamo[2], H. Vehkamäki[4], L. Sogacheva[4], and M. Kulmala[4]

[1]Department of Biological and Environmental Sciences, University of Helsinki, P.O. Box 27, 00014 Helsinki, Finland
[2]Finnish Meteorological Institute, P.O. Box 503, 00101 Helsinki, Finland
[3]Nordic Envicon Ltd., Koetilantie 3, 00790 Helsinki, Finland
[4]Department of Physical Sciences, University of Helsinki, P.O. Box 64, 00014 Helsinki, Finland

Received: 6 June 2006 – Accepted: 1 July 2006 – Published: 19 July 2006

Correspondence to: J. V. Niemi (jarkko.v.niemi@helsinki.fi)

Abstract

Aerosol samples were collected at a rural background site in southern Finland in May 2004. The elemental composition, morphology and mixing state of individual aerosol particles in three size fractions were studied using transmission electron microscopy (TEM) coupled with energy dispersive X-ray (EDX) microanalyses. The TEM/EDX results were complemented with the size-segregated bulk chemical measurements of selected ions and organic and elemental carbon. Many of the particles in $PM_{0.2-1}$ and $PM_{1-3.3}$ size fractions were strongly internally mixed with S, C and/or N. The major particle types in all $PM_{0.2-1}$ samples were ammonium sulphates with/without carbon and dark inclusion(s) (number proportion of particles 54–86%), carbon/sulphate mixture with dark inclusions(s) (4–10%), internally mixed soot/sulphate particles (2–22%), soot (0–12%) and K-rich particles with S and/or C (0–9%). During the pollution episode ($PM_{1.6}$~18 $\mu g\,m^{-3}$), the proportion of Ca-rich particles was very high (26–48%) in the $PM_{1-3.3}$ and $PM_{3.3-11}$ samples, while the $PM_{0.2-1}$ and $PM_{1-3.3}$ samples contained elevated proportions of silicates (22–33%, also fly ash particles), metal oxides/hydroxides (1–9%) and tar balls (1–4%). These aerosols originated mainly from polluted areas of Eastern Europe, and some open biomass burning smoke was also brought by long-range transport. During the clean period ($PM_{1.6}$~2 $\mu g\,m^{-3}$), when air masses arrived from the Arctic Ocean, $PM_{1-3.3}$ samples contained mainly sea salt particles (67–89%) with a variable rate of Cl substitution (mainly by NO_3^-). During the intermediate period ($PM_{1.6}$~5 $\mu g\,m^{-3}$), the $PM_{1-3.3}$sample contained porous (sponge-like) Na-rich particles (35%) with abundant S, K and O. They might originate from the burning of wood pulp wastes of paper industry. The proportion of biological particles and C-rich fragments (probably also biological origin) were highest in the $PM_{3.3-11}$ samples (0–81% and 0–22%, respectively). The origin of different particle types and the effect of aging processes on particle composition and their hygroscopic and optical properties are discussed.

ACPD

6, 6753–6799, 2006

1 Introduction

The composition and mass concentrations of fine aerosol particles ($PM_{2.5}$) in clean background areas are strongly affected by long-range transport. During transport and aging, particles of different origin may change their properties due to coagulation and cloud processes as well as due to reactions with gases via various heterogeneous pathways. Thus, differences in sources and in meteorological conditions may strongly affect composition, mixing state, concentration and size of different particle types observed. These are essential factors related to the environmental and health impacts of aerosols, such as climate change and transport of nutrients, acids and toxic compounds (EMEP, 2001; IPCC, 2001; WHO, 2003; Chung and Seinfeld, 2005; Kanakidou et al., 2005; Sun and Ariya, 2006).

In Finland, anthropogenic emissions of particles and their precursor gases are low (EMEP, 2001, 2002), and most of the $PM_{2.5}$ mass originates from long-range transport (Pakkanen et al., 2001; Vallius et al., 2003; Karppinen et al., 2004). In general, $PM_{2.5}$ concentrations are also low, the annual mean $PM_{2.5}$ concentration being only $5.8\,\mu g\,m^{-3}$ at the rural station of Hyytiälä in southern Finland (Laakso et al., 2003). However, the particle concentration and composition vary strongly depending on meteorological conditions and aerosol source regions. High particle mass concentrations are observed when air masses arrive from polluted continental areas of Central and Eastern Europe, and low concentrations when air masses originate from the direction of the Atlantic and Arctic Oceans (Pakkanen et al., 2001; Ricard et al., 2002; Ruoho-Airola et al., 2004; Sogacheva et al., 2005; Tunved et al., 2005). Thus, clean background areas in Finland are especially favourable for investigation of the properties of aged, long-range transported aerosols with clearly different origins.

The composition of aerosol particles has been studied mostly with bulk chemical methods. Only a few studies on background aerosols in continental Europe have been performed using individual particle methods (Ebert et al., 2002, 2004; Held et al., 2002; Hinz et al., 2005), and these studies are especially sparse for Northern Europe

(Bigg, 2001; Tervahattu et al., 2005). Individual particle methods provide information on chemical composition, sources, morphology and mixing state of particles, which cannot be observed with bulk chemical methods.

We examined the composition, morphology and mixing state of individual aerosol particles with the TEM/EDX method at a rural background site in southern Finland during polluted, intermediate and clean periods with different origins of particles. We describe major particle types observed in three size fractions ($PM_{0.2-1}$, $PM_{1-3.3}$ and $PM_{3.3-11}$) and investigate changes in their abundances, composition, mixing state and sources during different periods. To our knowledge, this is the first TEM/EDX study on background aerosols in continental Northern Europe. The results are compared with bulk chemical measurements performed during the same field campaign and also with individual particle studies for background aerosols conducted by other research groups. Furthermore, the effect of aging processes on particle composition and their hygroscopic and light absorption properties are discussed.

2 Materials and methods

2.1 Aerosol sampling

Aerosol samples were collected at the SMEAR II station (61.85 N, 24.28 E, 181 m a.s.l.) in Hyytiälä between 6 and 24 May 2004. The field station, located in a boreal pine forest, represents a clean background area in southern Finland (details in Kulmala et al., 2001).

Particle samples for bulk chemical analysis were collected with two identical virtual impactors (VIs) in parallel; one was used to collect samples for mass and ion analysis and the other for carbon analysis (Saarikoski et al., 2005). The VIs were modified versions of the original design of Loo and Cork (1988). They divide airborne particle matter into two size fractions: $PM_{1.3}$ and $PM_{1.3-10}$. Collection substrates for mass and ion analysis were Teflon filters (diameter 47 mm, pore size 3.0 μm, Millipore Fluoropore,

Ireland), and for carbon analysis quartz fibre filters (diameter 47 mm, Whatman QMA). In VI sampling for carbon analysis, denuders and back-up filters were used to minimize sampling artefacts. Sampling time was two days.

Particle samples for TEM/EDX individual particle analysis were collected with a Battelle-type impactor (model I-1, PIXE International Corporation, Florida, USA), which is a modified version of the original design of Mitchell and Pilcher (1959). Cu TEM grids (400-mesh) with carbon-coated Formvar films (Carbon Type-B, Ted Pella Inc., Redding, CA, USA) were placed on three impaction stages to collect particles in diameter ranges (cut-off sizes, D_{50}) of 0.2–1.0, 1.0–3.3 and 3.3–11 μm. The flow rate was 1 L/min. Sample collection times were 1–6 h, depending on the particle concentrations during sampling. The TEM grids of six sampling periods (6 periods and 3 size fractions, total 18 TEM grids) were used for TEM/EDX analysis.

2.2 Bulk chemical analysis

VI samples were analysed chemically for elemental carbon (EC), organic carbon (OC), water-soluble ions and the sum of three monosaccharide anhydrides ($\sum$MA = levoglucosan + galactosan + mannosan). EC and OC were measured with the thermal-optical carbon analyser (Sunset Laboratory Inc., Oregon, USA). Ion analysis was performed using two Dionex-500 ion chromatography systems, and the ions analysed were NO_3^-, SO_4^{2-}, Cl^-, methanesulphonate (MSA), oxalate, succinate, malonate, Na^+, NH_4^+, K^+, Mg^{2+} and Ca^{2+}. The details of ion and carbon analysis, and also the weighting of VI samples to calculate particle mass concentrations, are described in Saarikoski et al. (2005). $\sum$MA was determined by using a liquid chromatograph mass spectrometer (LC/MS; Agilent 1100 Series, Trap SL, Agilent Technologies, USA), and the analysis method is described in detail by Sillanpää et al. (2005).

2.3 TEM/EDX individual particle analyses

The morphology and elemental composition of individual aerosol particles were investigated using a Tecnai 12 transmission electron microscope (TEM) equipped with an EDAX energy dispersive X-ray (EDX) microanalyser. The TEM was operated on an accelerating voltage of 120 kV and with a low beam current to minimize beam damage. Counting time for X-ray spectra was 20 live seconds. The minimum size of particles analyzed was 0.2 μm (geometric diameter).

The elements analysed were with Z from C to Pb, excluding N. The X-ray counts from carbon-Formvar coating (thickness listed as ~60 nm; contains abundant C, some O and minor Si) of TEM grids were estimated by analysing blank areas between particles. The net X-ray counts (= total counts – carbon-Formvar blank counts) of elements for each particle analysed were calculated, and their proportions were normalized to 100%. Although the elemental results were semiquantitative, the accuracy is sufficient to identify different particle types and to compare the differences in elemental ratios of the same particle type in different samples (Pósfai et al., 2003; Ebert et al., 2004; Niemi et al., 2005b; Ro et al., 2005; Laskin et al., 2006). The strong vacuum (~10^{-7} torr) and beam exposure causes evaporation of semi-volatile compounds from particles, and for that reason, water, ammonium nitrate and organic compounds with high vapour pressure were lost, as is typical in electron microscopy.

2.4 Air quality and meteorological data

Temperature, relative humidity (RH), wind speed, wind direction and concentrations of gaseous components (O_3, CO, SO_2, NO_2 and NO) are recorded continuously at the SMEAR II station. Particle number concentrations and size distributions (from 29 nm to 10 μm) were monitored continuously during the field campaign (time resolution 1 s, averaged to 10 min) with Electrical Low Pressure Impactor (Outdoor Air ELPI, Dekati Ltd, Tampere, Finland), and these results were used to calculate $PM_{1.6}$ mass concentrations (equations described in Saarikoski et al., 2005). Backward air mass tra-

jectories were produced using the HYbrid Single-Particle Lagrangian Integrated Trajectory (HYSPLIT4) model (Draxler and Rolph, 2003) with the Final Analyses (FNL) meteorological database at the NOAA Air Resources Laboratory's web server (Rolph, 2003). The Navy Aerosol Analysis and Prediction System (NAAPS) model results were used to determine the distribution of smoke aerosols from open biomass burning (http://www.nrlmry.navy.mil/aerosol/; the Naval Research Laboratory, Monterey, CA, USA).

3 Results and discussion

3.1 Air quality and meteorology during sampling periods

The particle mass concentrations were high at the beginning of the field campaign, and the first two samples (6 and 7) for TEM/EDX analysis were collected during that pollution episode (Fig. 1 and Table 1). The hourly $PM_{1.6}$ mass reached 23 μg m^{-3} during the episode, which is 5 times higher than the mean spring-time PM_1 concentration in Hyytiälä (Laakso et al., 2003). During the episode, most of the PM_{10} mass was in the $PM_{1.3}$ size fraction (~80%), which is a slightly higher proportion than in the rest of the field campaign (~60–70%). The concentrations of gaseous pollutants were also unusually high. The maximum value (90 ppb) of O_3 concentration in 2004 was also observed during this episode. Elevated particle mass and O_3 concentrations were observed over larger areas in Finland between 4 and 9 May due to long-range transport of pollutants.

The backward trajectories show that during the pollution episode the continental air masses arrived from the direction of south-western Russia, Belarus and Ukraine (Fig. 2), which belong to typical source regions (polluted areas of Eastern and Central Europe) for aerosol particle episodes observed in Finland (Niemi et al., 2004, 2005a; Tervahattu et al., 2004; Sogacheva et al., 2005). During the episode, the weather was exceptionally warm (over +20°C, Table 1) compared with the mean temperature for

May (+9°C in that region in 1971–2001; Finnish Meteorological Institute). Only a few small showers occurred during the whole field campaign. The samples for TEM/EDX analysis were collected during the periods when there was no rain.

Sample 10 was collected just after or at the end of the pollution episode, and during that intermediate period (between the pollution episode and the clean period) the $PM_{1.6}$ concentration was 5.1 $\mu g\,m^{-3}$ (Fig. 1 and Table 1). The short backward trajectory of air masses originated from the north-east and curved towards the Arctic Ocean (Fig. 2). The last three samples (nos. 17–22) were collected during the clean period, when both $PM_{1.6}$ mass (2.0–2.6 $\mu g\,m^{-3}$) and gaseous component concentrations were very low. Air masses arrived in Finland from the Arctic Ocean, passing over Norway and Sweden, which is a typical source sector for low particle mass concentrations (Sogacheva et al., 2005) due to minor anthropogenic emissions.

3.2 Bulk chemical concentrations

The $PM_{1.3}$ and $PM_{1.3-10}$ concentrations for particle mass, ions, $\sum$MA, EC and OC are shown in Table 2. The results of bulk chemical analysis are not completely comparable with TEM/EDX results because of strong differences in the lengths of sampling periods (see difference in sampling periods with Battelle impactor for TEM/EDX and with VI for bulk chemical analysis in Fig. 1). However, the bulk chemical results give a good overview of particle composition during the sampling periods, with clearly different aerosol origins being apparent.

Most of the chemical components reached their maximum concentrations during the pollution episode (Table 2). During the clean period, the concentrations of Na^+, Cl^-, Mg^{2+} and MSA were elevated, which confirms the marine origin of the air mass. The concentrations of most chemical components were much higher in $PM_{1.3}$ samples than in $PM_{1.3-10}$ samples. However, NO_3^-, Cl^-, Na^+(not during pollution episode), Mg^{2+} and Ca^{2+} were mostly present in the $PM_{1.3-10}$ size fraction.

The main components in all $PM_{1.3}$ samples were OC, SO_4^{2-}, NH_4^+ and EC, their to-

tal proportions in the $PM_{1.3}$ mass being 73–83% (Table 2). The unidentified fraction was also quite high (20.0–25.5%), and its major components were probably unanalysed elements related to OC (especially O, H and N). During the pollution episode, the unidentified fraction was especially large (25.5%), and it also contained silicates and metal oxides/hydroxides, as will be shown in TEM/EDX results. The weight percentage of K^+ (0.90%) and oxalate (0.77%) and the concentration of monosaccharide anhydride ($\sum$MA=15 ng m^{-3}) also reached their peak values during the pollution episode, indicating the presence of biomass burning aerosols (Andreae, 1983; Andreae et al., 1998; Simoneit et al., 1999; Sillanpää et al., 2005). However, their concentrations only rose slightly (especially $\sum$MA), which suggests that biomass burning was one sources but not the main source of pollution episode aerosols. During a strong long-range transported wildfire smoke episode in Helsinki, Finland, the $\sum$MA concentrations reached over 20-fold higher values (365 ng m^{-3}) in three-day $PM_{2.5}$ samples (Sillanpää et al., 2005). Satellite observations (MODIS fire detections, Web Fire Mapper maps at http://maps.geog.umd.edu/) indicate that there were numerous fire areas, presumable agricultural field-burning and wildfires in Eastern Europe and especially in Russia, before and during the pollution episode. The trajectories (Fig. 2) and NAAPS model results (Fig. 3) indicate that some smoke aerosol from these fires arrived in Finland during this period.

The main components in all $PM_{1.3-10}$ samples were OC, EC, NO_3^- and SO_4^{2-} (Table 2). During the pollution episode, the weight percentages of Ca^{2+} (4.1%) and unidentified components (28.1%) were especially high. During the clean marine period, Na^+ and Cl^- weight percentages reached their highest proportions (7% and 9%, respectively, in the 20–22/05 sample).

3.3 Major particle types and their abundances by TEM/EDX

The individual particles analysed were classified into 12 different particle groups based on their elemental composition, morphology, internal structure and susceptibility to

damage by an electron beam. The particle groups and classification criteria are presented in Table 3. The relative abundances of each particle group in different size fractions are shown in Table 4. The particles of the first six groups were mostly present in $PM_{0.2-1}$ samples, and these particle types were 1) tar balls, 2) soot, 3) soot/sulphate mixture, 4) carbon/sulphate mixture with dark inclusion(s), 5) ammonium sulphates with/without carbon and dark inclusion(s) and 6) K-rich particles with S and/or C. The relative proportions of the remaining six particle groups were usually highest in either $PM_{1-3.3}$ or $PM_{3.3-11}$ samples; 7) Ca/Mg carbonates, sulphates and/or nitrates, 8) silicates, 9) metal oxides/hydroxides, 10) sea salt and other Na-rich particles, 11) biological particles and 12) C-rich fragments.

3.3.1 Tar balls

During the pollution episode, $PM_{0.2-1}$ and $PM_{1-3.3}$ samples contained some (1–4%) individual spherical C-rich particles that were very dark (electron-dense), amorphous and totally stable even in the presence of very strong electron beam (Fig. 4). Pósfai et al. (2003; 2004) named this kind of particles as tar balls, a distinct carbonaceous particle type from soot. Tar balls originate from biomass burning, especially during smouldering burning conditions (Pósfai et al., 2003, 2004; Chakrabarty et al., 2006). The relative proportion of the tar balls remained quite low or moderate (1–4% tar balls) during the pollution episode compared with the proportion observed at some other sites (Pósfai et al., 2003; Pósfai et al., 2004; Hand et al., 2005). The low proportion of tar balls is consistent with our bulk chemical results, indicating that biomass burning was one source but not the main source of the pollution episode.

The ternary diagrams in Fig. 5 show elemental ratios of tar balls in our samples. The most abundant elements were C (mean 84% of X-ray counts) and O (mean 11%). Furthermore, all particles contained some S (mean 4%), and half of the particles contained minor amounts of K (mean of all analysed particles 1%). In general, these elemental results are consistent with those of Pósfai et al. (2003, 2004) and Hand et al. (2005). However, they also observed Cl in some tar balls, and S was not present in all particles.

Thus, the tar balls in our samples were likely transported from a distant origin, probably from open fires in Eastern Europe (see Fig. 3), because Cl is absent and S is enriched in aged biomass smoke due to Cl depletion and accumulation of secondary products (Liu et al., 2000; Li et al., 2003b; Pósfai et al., 2003). The elemental results and visual inspection indicate that mixing with sulphate was very slight in tar balls compared with the mixing of soot with sulphate (next section). This observation is consistent with other studies (Pósfai et al., 2003, 2004; Hand et al., 2005). Tar balls scatter and absorb light strongly, and they do not exhibit deliquescence but do uptake some water at ~83% RH and may dissolve at higher RH (Hand et al., 2005). Thus, they may play an important role in regional haze and climate forcing.

3.3.2 Soot and mixed soot/sulphate particles

Soot particles and their mixtures with sulphate were common (total proportion 7–34%) in all $PM_{0.2-1}$ samples (Table 4). Soot particles are formed by numerous spherical carbon particles (diameter ~20–50 nm), and the morphology of soot varies from short chains to complex chain-agglomerates depending on burning conditions (Fig. 6a, Pósfai et al., 2003; Kocbach et al., 2005). The morphology of several soot aggregates was collapsed and compact, which suggests that they have been in contact with water during transport (Zuberi et al., 2005). Several soot particles were strongly mixed with beam-sensitive, S-containing material. The morphology of these internally mixed soot/sulphate particles varied strongly, and in some of these particles, soot had almost totally lost its characteristic morphology (Figs. 6b–d, see also Fig. 4).

In addition to C, O and variable S, most soot and mixed soot/sulphate particles contained also minor amounts of K and some particles contained small quantities of Si (Fig. 6g). These are typical minor elements in soot (Kocbach et al., 2005). The C-S-K ternary diagrams in Figs. 6e and f show the marked difference in S content of soot and soot/sulphate mixed particles. In $PM_{0.2-1}$ samples, ~60% (range 25–100%, see Table 4) of soot was internally mixed with sulphate. The strong internal mixing of soot is in line with other studies performed in clean background areas, far from soot emission

sources (Pósfai et al., 1999; Hasegawa and Ohta, 2002; Li et al., 2003a; Okada et al., 2005). While freshly emitted soot is extremely hydrophobic, the aging processes such as coagulation, condensation and chemical reactions cause soot to become more hydrophilic (Zuberi et al., 2005). The internal mixing of soot with sulphate (as well with hygroscopic OC and nitrate) particles strengthens soot's light absorption properties, increasing the direct radiative forcing (Chung and Seinfeld, 2005; Schnaiter et al., 2005). However, the total effect of soot on radiation balance of the Earth is still difficult to estimate accurately because the aging of soot decreases its poorly know surface area (see van Poppel et al., 2005 based on 3-dimensional TEM images), shortens its residence time in the atmosphere due to more efficient wet deposition and enables soot to act as cloud condensation nuclei (CCN) (Liu et al., 2005; Zuberi et al., 2005).

3.3.3 Beam-sensitive S-, C- and/or K-rich particles with/without dark inclusions

In addition to soot and mixed soot/sulphate particles, there were many other S- and/or C-rich particles without recognizable soot inclusions in $PM_{0.2-1}$ samples. Some of these particles also contained abundant K. These beam-sensitive particles were divided into following three groups based on their C, S and K content as well as morphology (Table 3): 1) mixed carbon/sulphate with dark inclusion(s), 2) ammonium sulphates with/without carbon and dark inclusion(s) and 3) K-rich particles with C and/or S. This classification is quite rough, but it is useful to describe some characteristics of these large particle groups of $PM_{0.2-1}$ samples (total proportion 61–94%, Table 4).

The "mixed carbon/sulphate with dark inclusion(s)" group contained particles with grey (= electron-transparent) beam-sensitive material and dark (= electron-opaque) beam-resistant fragments (Fig. 4). The proportion of C was high in these particles, and they also contained abundant S and O, often minor K and sometimes small amounts of other elements such as Mg, Ca, Na, Si and Al. The strong presence of C is illustrated in Fig. 7 by using a S-C-K ternary diagram. The proportion of this particle type was 4–10% in $PM_{0.2-1}$ samples (Table 4), which is quite similar to the proportions of soot (0–12%) and mixed soot/sulphate particles (2–22%). The origin of the dark inclusions in

this mixed carbon/sulphate group remained unclear. They might contain material from particles of biological origin and/or material from burning sources such as collapsed tar balls or soot.

The particles in the "ammonium sulphates with/without carbon and dark inclusion(s)" group were beam-sensitive (grey, electron-transparent material) and contained only rarely minor beam-resistant inclusions (dark, electron-opaque material) (see Fig. 4). The TEM/EDX results showed that these particles contained S and O. The sulphur was probably present as ammonium sulphate because the particles did not have a satellite droplet ring(s) around them, which is characteristic of such acid sulphates as H_2SO_4 particles (Pósfai and Molnár, 2000; Kojima et al., 2004, 2005). The high concentrations of NH_4^+ measured by ion chromatography (Table 2) also support the dominance of ammonium sulphate. "Ammonium sulphates with/without carbon and dark inclusion(s)" was the most significant (54–89%) particle group in all $PM_{0.2-1}$ samples (Table 4).

According to TEM/EDX results, ammonium sulphate particles were often mixed with variable amounts of C and minor K, and sometimes minor amounts of other elements such as Mg, Ca, Na, Si and Al. Furthermore, a few particles contained small quantities of Pb, Zn, V and Ni during the pollution episode. The elevated total C peak to background C peak ratios (>1.3) were considered rough estimates of the presence of detectable carbon in ammonium sulphate particles. Although the size and morphology of particles were fairly similar in all $PM_{0.2-1}$ samples, there were clear differences between samples in the proportion of particles with detectable C (Fig. 8). The results indicate that there were large amounts of particles with internally mixed ammonium sulphate and carbon; their proportions were higher during the pollution episode (34–43% in samples 6 and 7) and the intermediate period (58% in sample 10) than in the clean, marine period (11–19% in samples 17–22). The presence of internally mixed ammonium sulphate and carbon is in line with other recent studies, conducted in various continental environments (Lee et al., 2002; Pósfai et al., 2003; Dall'Osto et al., 2004; Tervahattu et al., 2005; Zhang et al., 2005). Pósfai and Molnár (2000) also show some visual evidence (TEM images) that ammonium sulphate particles are more

strongly mixed with carbon (thick coating residuals) in polluted continental samples than in clean marine samples. However, it is still insufficiently known what kind of mixtures ammonium sulphate and OC form in the atmosphere (e.g. composition and thickness of coatings and their evolution), how commonly these mixed particles exist and how strongly the changes in the mixing state affect the properties of the particles (e.g. impact on hygroscopic growth and reactions with gases) (Kanakidou et al., 2005; Donaldson and Vaida, 2006; Sun and Ariya, 2006).

The third S-K-C-containing particle group without typically characteristic morphology (such as soot or tar balls) was K-sulphates with/without carbon. They contained abundant beam-sensitive material and sometimes dark inclusions. The presence of K-rich particles with C and S is typical of aerosols originating from biomass burning. The proportion of these K-rich particles was 0–9% in $PM_{0.2-1}$ samples. The highest proportion (9%) was observed during the clean, marine period (sample 17). However, this might be a coincidence due to the relatively small number of particles analysed. There were slight differences between samples when K/S ratios were calculated for all S-C-K–rich particle groups, including all three particle groups discussed in this section as well as tar balls, soot and mixed soot/sulphate particles; the median K/S values were slightly higher during the pollution episode (0.21 and 0.16 for samples 6 and 7, respectively) and during the intermediate period (0.12 for sample 10) than during the clean, marine period (0.12, 0.8 and 0.5 for samples 17, 20 and 22, respectively). This indicates again the presence of some biomass-burning aerosols during the pollution episode. In sample 6, emissions from oil-shale-burning industrial areas, located in Narva (see Fig. 2) and Slantsy (~25 km south of Narva), may also have increased the K/S ratio because they contain a substantial amount of K in the submicron size range (Häsänen et al., 1997; Tervahattu et al., 2004).

3.3.4 Silicates and metal oxides/hydroxides

Si-O-rich particles with variable amounts of other typical elements of the Earth's crust (Al and minor Fe, Ca, K, Mg, Na and/or Ti depending on the mineralogy of particles)

were classified as silicates, while particles in the "metal oxides/hydroxides" group were mostly Fe-rich, and a few particles also contained abundant Zn, Mn and/or Pb. The shape of silicates and metal oxides/hydroxides was usually angular, but a few spherical fly ash particles were also observed. The proportions of both angular and spherical silicates and metal oxides/hydroxides were especially high during the pollution episode (Table 4), and Pb-containing particles were observed only during this period. When all particles with at least minor (detectable) Pb were counted from all particle groups (some S-K-C-rich particles also contained Pb as mentioned above), the proportions of Pb-containing particles were 3–7% in $PM_{1-3.3}$ and $PM_{0.2-1}$ samples. These elevated proportions of heavy metals and fly ash particles indicate that polluted air masses from Eastern Europe carried aerosols from metal industry and/or fossil fuel burning.

The silicates contained variable amounts of S, and the S proportions were clearly higher in $PM_{1-3.3}$ samples than in $PM_{3.3-11}$ samples (Figs. 9a and b). The proportion of silicates with a S/(Si+Al+S) ratio > 0.02 (see S=2% line in Figs. 9a and b) was 84% for $PM_{0.2-1}$ and $PM_{1-3.3}$ (merged) samples, and only 23% for $PM_{3.3-11}$ samples. This difference in S content probably results from the accumulation of sulphate on the surfaces of silicates during transport due to condensation and coagulation of S-containing species. The silicates in $PM_{1-3.3}$ samples have a higher surface area to volume ratio and a longer residence time in the atmosphere (due to slow gravitational removal) than larger silicate particles in $PM_{3.3-11}$ samples, which probably explains the difference in S proportion. The sulphate accumulation on the surface of the silicates increases their hygroscopicity and enables these internally mixed particles to act as CCN at high supersaturation.

3.3.5 Ca-rich particles

Ca-O-rich particles with variable Mg, C, S and Si were classified as Ca-rich particles (see example spectra in Figs. 10a and b). Furthermore, some of these particles contained minor amounts of other elements such as Al, K, P and Fe. The shape of the Ca-rich particles varied from angular to completely rounded (Figs. 10a and b). The

ratios of major elements in Ca-rich particles for different $PM_{1-3.3}$samples are shown in ternary diagrams (Fig. 10c). The dominance of Ca and C, with abundant Mg and/or Si in a few particles, suggests the presence of Ca- and Ca-Mg-carbonates (e.g. calcite $CaCO_3$ and dolomite $CaMg(CO_3)_2$) and their (minor) mixtures with silicates. Furthermore, S was detected in all particles, which indicates that they contained sulphate. Nitrate was also probably present because the proportions of C, S and Si were very low in some particles, and only Ca and O were detected. However, only very weak N peaks were observed in X-ray spectra due to strong peak overlap of C and O with N and due to the deep gap in transmissions characteristic of the EDX window for the Kα line of N.

The relative number of Ca-rich particles was very high during the pollution episode (samples 6–7), especially in $PM_{1-3.3}$ samples (39–48%) but also in $PM_{3.3-11}$ samples (26–28%). During other sampling periods, these size fractions contained ≤10% Ca-rich particles, and in $PM_{0.2-1}$ samples there were practically no Ca-rich particles. During the pollution episode, air masses passed over Estonian and Russian oil-shale-burning industrial areas located in Narva and Slantsy (sample 6, see Fig. 2), and over the region of St. Petersburg (sample 7). These regions belong to the strongest source areas of aerosols and Ca in Northern Europe (Häsänen et al., 1997; Lee and Pacyna, 1999; Jalkanen et al., 2000; EMEP, 2002), and thus, the pollution episode Ca-rich particles might originate mainly from these areas. A more detailed source identification of Ca-rich particles is difficult because they can originate from various sources, including fossil fuel and biomass burning, cement and metal industries, soil dust and marine sources (Hoornaert et al., 1996; Lee and Pacyna, 1999; Li et al., 2003b). However, the relative amount of Mg and Si in Ca-rich particles was highest in sample 6 and lowest in samples 10-22 (see Fig. 10c), which can be explained by the differences in their origin. For instance, the proportion of particles with Ca/(Ca+Mg+Si)>80% (see Si-Ca-Mg ternary diagrams in Fig. 10c) were 24% for sample 6, 59% for sample 7 and 70% for samples 10–22. The high proportion of Ca-rich particles with only minor Si and/or Mg in samples 10–22 might indicate a stronger impact of such marine sources

as fractional recrystallization of sea salt particles or marine organisms (e.g. coccoliths) (Andreae et al., 1986).

The substitution of CO_3^{2-} by SO_4^{2-} and NO_3^- is typical of Ca/Mg carbonates in the atmosphere due to reactions with SO_2 and HNO_3 (Song and Carmichael, 1999; Al-Hosney and Grassian, 2005; Laskin et al., 2005b). These conversion products are highly hygroscopic (e.g. deliquescence RH for amorphous $Ca(NO_3)_2$ particles is only ~13%, Tang and Fung, 1997). In $PM_{1-3.3}$ samples, several rounded Ca-rich particles seemed to be very thin (light contrast in TEM images), indicating that they have been in liquid form during the impaction on TEM grids. During the collection of samples 6–7, the RH was only 30–31%, which shows that also mixed Ca/Mg carbonates/sulphates/nitrates may occur at least partly in liquid form even at very low RH. This is consistent with the results of recent laboratory studies with environmental SEM (with adjustable RH) for Ca-rich particles collected from various environments (Laskin et al., 2005a, 2005b). The substitution of CO_3^- with SO_4^{2-} and NO_3^- from Ca/Mg-rich particles may change optical and CCN properties as well as residence time in the atmosphere. Furthermore, these reactions provide a sink for SO_2 and HNO_3 and release CO_2.

3.3.6 Sea salt and other Na-rich particles

The morphology and composition of sea salt particles varied strongly. They contained abundant Na and variable amounts of Cl and/or S and O, depending on the rate of Cl substitution, as well as minor amounts of Mg, Ca and K. There were cubic, angular and rounded particles, and some of them contained cation (Ca, Mg and/or K) sulphate rims and rods. Images of sea salt particles with similar morphology and composition have been shown in several recent electron microscopy studies (e.g. Ebert et al., 2000; Li et al., 2003a). However, $PM_{1-3.3}$ sample 10 contained ordinary sea salt particles (36% of all analysed particles) and also other Na-rich particles without characteristic morphology and Mg-Ca-K ratios of sea salt (35% of all analysed particles). The morphology of the Na-rich particles was rounded and porous (sponge-like), and they seemed to

be composed of numerous, small spherical subparticles (Fig. 11a particles no. 2 and Fig. 11b). They were not very sensitive to beam damage, but under strong intentional beam exposure they were damaged slightly, similarly to sea salt particles. These porous particles contained abundant Na and O and some S and K, while Mg and Ca were (almost) totally absent (compare spectra in Figs. 11c and d). Ternary diagrams in Fig. 12 (diagrams in the bottom row) confirm the clearly deviating Mg-Ca-K ratios of these porous particles compared with sea salt particles, although there were also a few (non-porous) sea salt particles with deviating elemental ratios, probably due to inaccuracy in elemental analysis and potentially to the minor presence of fractional crystallization products. The median Mg/Na, K/Na and Ca/Na ratios were 0.131, 0.035 and 0.038, respectively, for all sea salt particles in $PM_{1-3.3}$ samples 10–22, while the corresponding values for Na-S-K-O-rich porous particles were 0.013, 0.141 and 0.004 in $PM_{1-3.3}$ sample 10. There were also some Na-rich particles with deviating Mg-Ca-K ratios in other samples, but their morphology was never porous.

The porous morphology of Na-S-K-O-rich particles strongly suggests that they were not of marine origin. During their sampling (sample 10), air masses had passed over paper industry areas located ~100 km northeast of Hyytiälä. Large amounts of sodium sulphate (Na_2SO_4) are used in wood pulp processing, and residuals from these processes are burned. Thus, the burning of mixed sodium sulphate and biomass residuals (contains abundant K) might be the source of Na-S-K-O-rich particles. However, burning of other waste is also a potential source for these particles (Hwang and Ro, 2006), because waste burning is a major source of Na in continental areas (Ooki et al., 2002). The plentiful presence of aerosols originated from burning sources in sample 10 is also supported by the high proportions of soot and mixed soot/sulphate particles in the $PM_{0.2-1}$ size fraction (12% and 22%, respectively, see Table 4) as well as by the elevated NO_2 and NO concentrations (Table 1). The Na-S-K-O-rich particles may have originally contained Cl (Na-Cl/S-K-O-rich particles), but the Cl substitution by sulphate (or by other acid anions) could have removed it during transport.

During the collection of sample 10, the trajectories curved towards the Arctic Ocean,

and in addition to Na-S-K-O-rich particles, abundant sea salt particles were present (37% in $PM_{1-3.3}$ sample), as mentioned above. Two hours after the sampling period, the back trajectories reached the Arctic Ocean, and thus, the presence of sea salt particles in sample 10 might indicate a slight inaccuracy in these strongly curved trajectories. A few sea salt particles were also present during the pollution episode (4–9% in $PM_{1-3.3}$ samples), but they are not shown in ternary diagrams due to the small amount of particles analysed. The relative proportions of sea salt particles rose especially high during the clean period (67–89% in $PM_{1-3.3}$ samples 17-22), when air masses arrived from the direction of the Arctic Ocean. Sea salt particles were also present in $PM_{3.3-11}$ samples (0–25%), but in $PM_{0.2-1}$ samples their abundance was invariably very low (0–3%).

The rate of Cl depletion varied strongly between samples (Fig. 12, ternary diagrams of Cl-Na-S ratios in the top row). The proportion of sea salt particles with strong Cl depletion (Cl/Na X-ray count ratio <0.2) was clearly highest (91%) in sample 10, while sample 20 contained mainly unreacted sea salt and only a few (4%) particles with strong Cl depletion. Samples 17 and 22 contained sea salt particles both with no/minor depletion and with strong Cl depletion (particles with strong depletion 40% and 34%, respectively). The main reasons for the especially strong Cl depletion in sample 10 were probably the long time spent over continent (see trajectory in Fig. 2) and the elevated concentrations of gaseous pollutants. The trajectory of sample 20 clearly stayed the shortest time above the continent before its arrival to Hyytiälä, and the concentrations of gaseous pollutants were very low. This explains well the low rate of Cl depletion in this sample.

Only a minor fraction of Cl was replaced with sulphate or MSA in all $PM_{1-3.3}$ samples since the S/Na was almost constant for most of the sea salt particles (Fig. 12, ternary diagrams in the top row). This suggests that Cl was replaced mainly by NO_3^-, which is usually the most important Cl-substituting anion together with SO_4^{2-} (Kerminen et al., 1997, 1998). Only a few very small X-ray count peaks for N were observed in the X-ray spectra due to the insensitivity of EDX to detect N. However, the presence of

NO_3^- is supported by the bulk chemical results since NO_3^- and SO_4^{2-} were the most common anions in $PM_{1.3-10}$ samples (Table 2). The Cl substitution by nitrate strongly changes the hygroscopic properties of salt-salt particles; $NaNO_3$ may contain liquid water at much lower RHs than unreacted sea salt particles (Hoffman et al., 2004). Thus, modification of sea salt particles may change their size, light scattering properties and affinity for CCN formation. The presence of water on sea salt surfaces also greatly enhances their reactivity with gases compared with dry sea salt (ten Brink, 1998; Hara et al., 2002). Furthermore, the nitrate and the non-sea salt SO_4^{2-} that accumulate into sea salt particles are removed rapidly from the atmosphere due to the large sizes of particles, which reduces the amounts of scavenged species in the atmosphere.

3.3.7 Biological particles and C-rich fragments

The biological particles contained abundant C, some O and variable amounts of K and/or P. Furthermore, a few particles also contained small quantities of Cl, S, Ca, Mg, Na, Si and/or Al. The morphology of these particles varied strongly from spherical and oval to complicated biological structures (Figs. 13a and c). Most of the biological particles were likely spores or conidia of fungi (Wittmaack et al., 2005), but the detailed classification of these particles was beyond the scope of this work. There were also several angular C-rich particles without clearly characteristic morphology of biological particles (Figs. 13b and d), and due to uncertainty in source identification, they were referred to as C-rich fragments. In addition to C, they contained some/minor O, but usually no P or K. The proportion of particles with detectable P or K was only 15% for C-rich carbon fragments, while the corresponding value for biological particles was 93% (compare also ternary diagrams for C-P-K ratios in Figs. 13e and f). The TEM images of C-rich fragments were usually quite light (low contrast), which suggests that the fragments were thin. Their appearance and composition further suggest that they might be abrasion products from the surfaces of living or dead organisms. If the C-rich fragments were of biological origin, our observations emphasize that there are abun-

dant biological particles that cannot be detected using only elemental ratios (as used in some computer-controlled SEM/EDX and EPMA studies), and visual observations are needed to separate them from other carbonaceous particles.

The proportions of biological particles and C-rich fragments were highest in the coarse size fraction (in $PM_{1-3.3}$ samples and especially in $PM_{3.3-11}$ samples), which is in line with other individual particle studies related to continental background aerosol composition in Northern Europe (Ebert et al., 2000, 2004). No clear difference was observed in the proportions of biological particles and C-rich fragments related to source regions of the air masses. They might originate mainly from local forests, but transport from more distant regions is also possible, as strong changes were seen in the presence of Ca-rich and sea salt particles.

4 Summary and conclusions

Aerosol samples were collected at a rural site in southern Finland during polluted, intermediate and clean periods with different origins of particles. The composition, morphology and mixing state of individual particles in three size fractions ($PM_{0.2-1}$, $PM_{1-3.3}$ and $PM_{3.3-11}$) were studied using the TEM/EDX method. TEM/EDX results were complemented with the size-segregated bulk chemical measurements of organic and elemental carbon and selected ions. For more detailed characterization and comparisons, the individual particles analysed were classified into the following 12 groups: 1) tar balls, 2) soot, 3) soot/sulphate mixture, 4) carbon/sulphate mixture with dark inclusion(s), 5) ammonium sulphates with/without carbon and dark inclusion(s), 6) K-rich particles with S and/or C, 7) Ca/Mg carbonates, sulphates and/or nitrates, 8) silicates, 9) metal oxides/hydroxides, 10) sea salt and other Na-rich particles, 11) biological particles and 12) C-rich fragments.

The composition, morphology and mixing state of particles varied strongly in different size fractions and during different sampling periods, depending on source areas of air masses. During the pollution episode ($PM_{1.6}$~$18\,\mu g\,m^{-3}$), aerosols originated mainly

ACPD
6, 6753–6799, 2006

from polluted areas of Eastern Europe, and some open biomass burning smoke was also brought by long-range transport. The proportions of the following particle types were increased: silicates and metal hydroxides/oxides with spherical morphology (fly ash), Pb-containing particles, tar balls and Ca/Mg carbonates/sulphates/nitrates. During the intermediate period ($PM_{1.6}$ ~5 $\mu g\,m^{-3}$), the backward air mass trajectories were short and curving towards the Arctic Ocean, and in $PM_{1-3.3}$ samples, there were abundant sea salt particles (36%) with strong Cl depletion and other porous (sponge-like) Na-rich particles (35%). The porous Na-rich particles contained abundant S, K and O, and practically no Mg and Ca. They might originate from waste burning, especially from the burning of wood pulp wastes of the paper industry, when Na-rich salts (Na_2SO_4) are used in processes. During the clean period ($PM_{1.6}$~2 $\mu g\,m^{-3}$), when air masses arrived from the Arctic Ocean, $PM_{1-3.3}$ samples contained abundant sea salt particles (67–89%). The rate of Cl depletion (mainly by NO_3^-) from sea salt varied markedly depending on the time spent over continent. Strong changes in particle composition were observed in the $PM_{1-3.3}$ size fraction during the different sampling periods. Thus, not only accumulation mode particles ($PM_{0.2-1}$) but also the finest coarse particles ($PM_{1-3.3}$) may originate mostly from remote sources in clean rural areas.

In all $PM_{0.2-1}$ samples, the major particle types observed were ammonium sulphates with/without carbon and dark inclusion(s) (proportion 54–86%), carbon/sulphate mixture with dark inclusions(s) (4–10%), internally mixed soot/sulphate particles (2–22%), soot (0–12%) and K-rich particles with S and/or C (0–9%). The strong mixing of C and S was typical for most particle types (excluding tar balls) in that size fraction. Furthermore, ammonium sulphate particles might be more frequently/strongly mixed with (vacuum- and beam-resistant) carbonaceous material in aerosols with clearly continental (anthropogenic) origin compared to more marine (clean) origin. The internal mixing of silicates with S was greater in small particles ($PM_{0.2-1}$ and $PM_{1-3.3}$) than in larger particles ($PM_{3.3.-11}$), probably indicating the accumulation of S during transport. Both Ca/Mg-rich particles and sea salt particles were strongly mixed with SO_4^{2-} and/or nitrate. The mixing state of particles changes their hygroscopic and optical properties,

ACPD
6, 6753–6799, 2006

thus affecting their direct and indirect radiative forcing and their reactivity with gaseous components.

Acknowledgements. The Helsinki University Environmental Research Centre, the Finnish Cultural Foundation and the Academy of Finland (contract no. 201131) are acknowledged for funding this study. We thank our colleagues at the following institutes for their collaboration: P. Aalto, V. Hiltunen, M. Boy and J. Martikainen (Department of Physical Sciences, University of Helsinki), M. Räisänen (The Geological Survey of Finland) and K. Kupiainen (Nordic Envicon Ltd.). The authors gratefully acknowledge the NOAA Air Resources Laboratory (ARL) for provision of the HYSPLIT transport and dispersion model and the READY website (http://www.arl.noaa.gov/ready.html) used in this publication. The Naval Research Laboratory is acknowledged for the NAAPS model results (website at http://www.nrlmry.navy.mil/aerosol).

References

Al-Hosney, H. A. and Grassian, V. H.: Water, sulfur dioxide and nitric acid adsorption on calcium carbonate: A transmission and ATR-FTIR study, Phys. Chem. Chem. Phys., 7, 1266–1276, 2005.

Andreae, M. O.: Soot carbon and excess fine potassium: Long-range transport of combustion derived aerosols, Science, 220, 1148–1151, 1983.

Andreae, M. O., Charlson, R. J., Bruynseels, F., Storms, H., Van Grieken, R., and Maenhaut, W.: Internal mixture of sea salt, silicates, and excess sulfate in marine aerosols, Science, 232, 1620–1623, 1986.

Andreae, M. O., Andreae, T. W., Annegarn, H., Beer, J., Cachier, H., le Canut, P., Elbert, W., Maenhaut, W., Salma, I., Wienhold, F. G., and Zenker, T.: Airborne studies of aerosol emissions from savanna fires in southern Africa: 2. Aerosol chemical composition, J. Geophys. Res., 103, 32 119–32 128, 1998.

Bigg, E. K.: The aerosol in a boreal forest in spring, Tellus B, 53, 510–519, 2001.

Chakrabarty, R. K., Moosmüller, H., Garro, M. A., Arnott, W. P., Walker, J., Susott, R. A., Babbitt, R. E., Wold, C. E., Lincoln, E. N., and Hao, W. M.: Emissions from the laboratory combustion of wildland fuels: Particle morphology and size, J. Geophys. Res., 111, D07204, doi:10.1029/2005JD006659, 2006.

Chung, S. H. and Seinfeld, J. H.: Climate response of direct radiative forcing of anthropogenic black carbon, J. Geophys. Res., 110, D11102, doi:10.1029/2004JD005441, 2005.
Dall'Osto, M., Beddows, D. C. S., Kinnersley, R. P., Harrison, R. M., Donovan, R. J., and Heal, M. R.: Characterization of individual airborne particles by using aerosol time-of-flight mass spectrometry at Mace Head, Ireland, J. Geophys. Res., 109, D21302, doi:101029/2004JD004747, 2004.
Donaldson, D. J. and Vaida, V.: The influence of organic films at the air-aqueous boundary on atmospheric processes, Chem. Rev., 106, 1445–1461, 2006.
Draxler, R. R. and Rolph, G. D.: HYSPLIT (HYbrid Single-Particle Lagrangian Integrated Trajectory). Model access via NOAA ARL READY Website (http://www.arl.noaa.gov/ready/hysplit4.html), NOAA Air Resources Laboratory, Silver Spring, MD., 2003.
Ebert, M., Weinbruch, S., Hoffmann, P., and Ortner, H. M.: Chemical characterization of North Sea aerosol particles, J. Aerosol. Sci., 31, 613–632, 2000.
Ebert, M., Weinbruch, S., Rausch, A., Gorzawski, G., Hoffmann, P., Wex, H., and Helas, G.: Complex refractive index of aerosols during LACE 98 as derived from the analysis of individual particles, J. Geophys. Res., 107, 8121, doi:10.1029/2000JD000195, 2002.
Ebert, M., Weinbruch, S., Hoffmann, P., and Ortner, H. M.: The chemical composition and complex refractive index of rural and urban influenced aerosols determined by individual particle analysis, Atmos. Environ., 38, 6531–6545, 2004.
EMEP: Transboundary acidification and eutrophication and ground level ozone in Europe. Joint CIAM & CCC & MSC-W report, EMEP Summary Report 1/2001, 2001.
EMEP: Transboundary particulate matter in Europe: Status Report 2002, EMEP Report 5/2002, 89 pp., 2002.
Hand, J. L., Malm, W. C., Laskin, A., Day, D., Lee, T., Wang, C., Carrico, C., Carrillo, J., Cowin, J. P., Collett, J., and Iedema, M.J.: Optical, physical, and chemical properties of tar balls observed during the Yosemite Aerosol Characterization Study, J. Geophys. Res., 110, D21210, doi:10.1029/2004JD005728, 2005.
Hara, K., Osada, K., Nishita, C., Yamagata, S., Yamanocuhi, T., Herber, A., Matsunaga, K., Iwasaka, Y., Nagatani, M., and Nakata, H.: Vertical variations of sea-salt modification in the boundary layer of spring Arctic during the ASTAR 2000 campaign, Tellus B, 54, 361–376, 2002.
Häsänen, E., AunelaTapola, L., Kinnunen, V., Larjava, K., Mehtonen, A., Salmikangas, T., Leskelä, J., and Loosaar, J.: Emission factors and annual emissions of bulk and trace ele-

ments from oil shale fueled power plants, Sci. Total Environ., 198, 1–12, 1997.
Hasegawa, S. and Ohta, S.: Some measurements of the mixing state of soot-containing particles at urban and non-urban sites, Atmos. Environ., 36, 3899–3908, 2002.
Held, A., Hinz, K. P., Trimborn, A., Spengler, B., and Klemm, O.: Chemical classes of atmospheric aerosol particles at a rural site in Central Europe during winter, J. Aerosol. Sci., 33, 581–594, 2002.
Hinz, K. P., Trimborn, A., Weingartner, E., Henning, S., Baltensperger, U., and Spengler, B.: Aerosol single particle composition at the Jungfraujoch, J. Aerosol. Sci., 36, 123–145, 2005.
Hoffman, R. C., Laskin, A., and Finlayson-Pitts, B. J.: Sodium nitrate particles: physical and chemical properties during hydration and dehydration, and implications for aged sea salt aerosols, J. Aerosol. Sci., 35, 869–887, 2004.
Hoornaert, S., Van Malderen, H., and Van Grieken, R.: Gypsum and other calcium-rich aerosol particles above the North Sea, Environ. Sci. Technol., 30, 1515–1520, 1996.
Hwang, H. and Ro, C.-U.: Single-particle characterization of municipal solid waste (MSW) ash particles using low-Z particle electron probe X-ray microanalysis, Atmos. Environ., 40, 2873–2881, 2006.
IPCC: Climate Change 2001 – The Scientific Basis, Cambridge University Press, New York, 289–348, 2001.
Jalkanen, L., Makinen, A., Häsänen, E., and Juhanoja, J.: The effect of large anthropogenic particulate emissions on atmospheric aerosols, deposition and bioindicators in the eastern Gulf of Finland region, Sci. Total Environ., 262, 123–136, 2000.
Kanakidou, M. Seinfeld, J. H., Pandis, S. N., et al.: Organic aerosol and global climate modelling: a review, Atmos. Chem. Phys, 5, 1053–1123, 2005.
Karppinen, A., Härkönen, J., Kukkonen, J., Aarnio, P., and Koskentalo, T.: Statistical model for assessing the portion of fine particulate matter transported regionally and long range to urban air, Scandinavian Journal of Work, Environ. Health, 30, 47–53, 2004.
Kerminen, V.-M., Pakkanen, T. A., and Hillamo, R. E.: Interactions between inorganic trace gases and supermicrometer particles at a coastal site, Atmos. Environ., 31, 2753–2765, 1997.
Kerminen, V.-M., Teinilä, K., Hillamo, R., and Pakkanen, T.: Substitution of chloride in sea-salt particles by inorganic and organic anions, J. Aerosol. Sci., 29, 929–942, 1998.
Kocbach, A., Johansen, B. V., Schwarze, P. E., and Namork, E.: Analytical electron microscopy of combustion particles: a comparison of vehicle exhaust and residential wood smoke, Sci.

Total Environ., 346, 231–243, 2005.
Kojima, T., Buseck, P. R., Wilson, J. C., Reeves, J. M., and Mahoney, M. J.: Aerosol particles from tropical convective systems: Cloud tops and cirrus anvils, J. Geophys. Res., 109, D12201, doi:10.1029/2003JD004504, 2004.
Kojima, T., Buseck, P. R., and Reeves, J. M.: Aerosol particles from tropical convective systems: 2. Cloud bases. J. Geophys. Res., 110, D09203, doi:10.1029/2004JD005173, 2005.
Kulmala, M., Hämeri, K., Aalto, P. P., Mäkelä, J. M., Pirjola, L., Nilsson, E. D., Buzorius, G., Rannik, Ü., Dal Maso, M., Seidl, W., Hoffman, T., Janson, R., Hansson, H. C., Viisanen, Y., Laaksonen, A., and O'Dowd, C. D.: Overview of the international project on biogenic aerosol formation in the boreal forest (BIOFOR), Tellus B, 53, 324–343, 2001.
Laakso, L., Hussein, T., Aarnio, P., Komppula, M., Hiltunen, V., Viisanen, Y., and Kulmala, M.: Diurnal and annual characteristics of particle mass and number concentrations in urban, rural and Arctic environments in Finland, Atmos. Environ., 37, 2629–2641, 2003.
Laskin, A., Iedema, M. J., Ichkovich, A., Graber, E. R., Taraniuk, I., and Rudich, Y.: Direct observation of completely processed calcium carbonate dust particles, Faraday Discuss., 130, 453–468, 2005a.
Laskin, A., Wietsma, T. W., Krueger, B. J., and Grassian, V. H.: Heterogeneous chemistry of individual mineral dust particles with nitric acid: A combined CCSEM/EDX, ESEM, and ICP-MS study, J. Geophys. Res., 110, D10208, doi:10.1029/2004JD005206, 2005b.
Laskin, A., Cowin, J. P., and Iedema, M. J.: Analysis of individual environmental particles using modern methods of electron microscopy and X-ray microanalysis, J. Electron Spectrosc. Relat. Phenom., 150, 260–274, 2006.
Lee, D. S. and Pacyna, J. M.: An industrial emissions inventory of calcium for Europe, Atmos. Environ., 33, 1687–1697, 1999.
Lee, S. H., Murphy, D. M., Thomson, D. S., and Middlebrook, A. M.: Chemical components of single particles measured with Particle Analysis by Laser Mass Spectrometry (PALMS) during the Atlanta SuperSite Project: Focus on organic/sulfate, lead, soot, and mineral particles, J. Geophys. Res., 107(D1), 4003, doi:10.1029/2000JD000011, 2002.
Li, J., Anderson, J. R., and Buseck, P. R.: TEM study of aerosol particles from clean and polluted marine boundary layers over the North Atlantic, J. Geophys. Res., 108, 4189, doi:10.1029/2002JD002106, 2003a.
Li, J., Pósfai, M., Hobbs, P. V., and Buseck, P. R.: Individual aerosol particles from biomass burning in southern Africa: 2, Compositions and aging of inorganic particles, J. Geophys.

Res., 108, 8484, doi:10.1029/2002JD002310, 2003b.
Liu, X. D., Van Espen, P., Adams, F., Cafmeyer, J., and Maenhaut, W.: Biomass burning in southern Africa: Individual particle characterization of atmospheric aerosols and savanna fire samples, J. Atmos. Chem., 36, 135–155, 2000.
Liu, X. H., Penner, J. E., and Herzog, M.: Global modeling of aerosol dynamics: Model description, evaluation, and interactions between sulfate and nonsulfate aerosols, J. Geophys. Res., 110, D18206, doi:101029/2004JD005674, 2005.
Loo, B. W. and Cork, C. P.: Development of high-efficiency virtual impactors, Aerosol Sci. Technol., 9, 167–176, 1988.
Mitchell, R. I. and Pilcher, J. M.: Improved cascade impactor for measuring aerosol particle sizes, Ind. Eng. Chem., 51, 1039–1042, 1959.
Niemi, J. V., Tervahattu, H., Vehkamäki, H., Kulmala, M., Koskentalo, T., Sillanpää, M., and Rantamäki, M.: Characterization and source identification of a fine particle episode in Finland, Atmos. Environ., 38, 5003–5012, 2004.
Niemi, J. V., Tervahattu, H., Vehkamäki, H., Martikainen, J., Laakso, L., Kulmala, M., Aarnio, P., Koskentalo, T., Sillanpää, M., and Makkonen, U.: Characterization of aerosol particle episodes in Finland caused by wildfires in Eastern Europe, Atmos. Chem. Phys, 5, 2299–2310, 2005a.
Niemi, J. V., Tervahattu, H., Virkkula, A., Hillamo, R., Teinilä, K., Koponen, I. K., and Kulmala, M.: Continental impact on marine boundary layer coarse particles on Atlantic Ocean between Europe and Antarctica, Atmos. Res., 75, 301–321, 2005b.
Okada, K., Ikegami, M., Zaizen, Y., Tsutsumi, Y., Makino, Y., Jensen, J. B., and Gras, J. L.: Soot particles in the free troposphere over Australia, Atmos. Environ., 39, 5079–5089, 2005.
Ooki, A., Uematsu, M., Miura, K., and Nakae, S.: Sources of sodium in atmospheric fine particles, Atmos. Environ., 36, 4367–4374, 2002.
Pakkanen, T. A., Loukkola, K., Korhonen, C. H., Aurela, M., Makela, T., Hillamo, R. E., Aarnio, P., Koskentalo, T., Kousa, A., and Maenhaut, W.: Sources and chemical composition of atmospheric fine and coarse particles in the Helsinki area, Atmos. Environ., 35, 5381–5391, 2001.
Pósfai, M., Anderson, J. R., Buseck, P. R., and Sievering, H.: Soot and sulfate aerosol particles in the remote marine troposphere, J. Geophys. Res., 104, 21 685–21 693, 1999.
Pósfai, M. and Molnár, A.: Aerosol particles in the troposphere: a mineralogical introduction, in: Environmental Mineralogy, edited by: Vaughan, D. and Wogelius, R., European Mineralogical

Union Notes in Mineralogy Vol 2. Eötvös Unversity Press, Budapest, 197–252, 2000.
Pósfai, M., Simonics, R., Li, J., Hobbs, P. V., and Buseck, P. R.: Individual aerosol particles from biomass burning in southern Africa: 1. Compositions and size distributions of carbonaceous particles, J. Geophys. Res., 108, 8483, doi:10.1029/2002JD002291, 2003.
Pósfai, M., Gelencser, A., Simonics, R., Arato, K., Li, J., Hobbs, P. V., and Buseck, P. R.: Atmospheric tar balls: Particles from biomass and biofuel burning, J. Geophys. Res., 109, D06213, doi:10.1029/2003JD004169, 2004.
Ricard, V., Jaffrezo, J. L., Kerminen, V. M., Hillamo, R. E., Sillanpää, M., Ruellan, S., Liousse, C., and Cachier, H.: Two years of continuous aerosol measurements in northern Finland, J. Geophys. Res., 107, 4129, doi:10.1029/2001JD000952, 2002.
Ro, C. U., Hwang, H., Chun, Y., and Van Grieken, R.: Single-particle characterization of four "Asian Dust" samples collected in Korea, using low-Z particle electron probe X-ray microanalysis, Environ. Sci. Technol., 39, 1409–1419, 2005.
Rolph, G. D.: Real-time Environmental Applications and Display sYstem (READY) Website (http://www.arl.noaa.gov/ready/hysplit4.html), NOAA Air Resources Laboratory, Silver Spring, MD., 2003.
Ruoho-Airola, T., Anttila, P., and Salmi, T.: Airborne sulfur and nitrogen in Finland - trends and exposure in relation to air transport sector, J. Environ. Monit., 6, 1–11, 2004.
Saarikoski, S., Mäkelä, T., Hillamo, R., Aalto, P. P., Kerminen, V.-M., and Kulmala, M.: Physico-chemical characterization and mass closure of size-segregated atmospheric aerosols in Hyytiälä, Finland, Boreal Env. Res., 10, 385–400, 2005.
Schnaiter, M., Linke, C., Möhler, O., Naumann, K. H., Saathoff, H., Wagner, R., Schurath, U., and Wehner, B.: Absorption amplification of black carbon internally mixed with secondary organic aerosol, J. Geophys. Res., 110, D19204, doi:10.1029/2005JD006046, 2005.
Sillanpää, M., Saarikoski, S., Hillamo, R., Pennanen, A., Makkonen, U., Spolnik, Z., Van Grieken, R., Koskentalo, T., and Salonen, R. O.: Chemical composition, mass size distribution and source analysis of long-range transported wildfire smokes in Helsinki, Sci. Total Environ., 350, 119–135, 2005.
Simoneit, B. R. T., Schauer, J. J., Nolte, C. G., Oros, D. R., Elias, V. O., Fraser, M. P., Rogge, W. F., and Cass, G. R.: Levoglucosan, a tracer for cellulose in biomass burning and atmospheric particles, Atmos. Environ., 33, 173–182, 1999.
Sogacheva, L., Dal Maso, M., Kerminen, V.-M., and Kulmala, M.: Probability of nucleation events and aerosol particle concentration in different air mass types arriving at Hyytiälä,

southern Finland, based on back trajectories analysis, Boreal Env. Res., 10, 479–491, 2005.
Song, C. H. and Carmichael, G. R.: The aging process of naturally emitted aerosol (sea-salt and mineral aerosol) during long range transport, Atmos. Environ., 33, 2203–2218, 1999.
Sun, J. and Ariya, P. A.: Atmospheric organic and bio-aerosols as cloud condensation nuclei (CCN): A review, Atmos. Environ., 40, 795–820, 2006.
Tang, I. N. and Fung, K. H.: Hydration and Raman scattering studies of levitated microparticles: $Ba(NO_3)_2$, $Sr(NO_3)_2$, and $Ca(NO_3)_2$, J. Chem. Phys., 106, 1653–1660, 1997.
ten Brink, H. M.: Reactive uptake of HNO3 and H2SO4 in sea-salt (NaCl) particles, J. Aerosol. Sci., 29, 57–64, 1998.
Tervahattu, H., Hongisto, M., Aarnio, P., Kupiainen, K., and Sillanpää, M.: Composition and origins of aerosol during a high PM_{10} episode in Finland, Boreal Env. Res., 9, 335–345, 2004.
Tervahattu, H., Juhanoja, J., Vaida, V., Tuck, A. F., Niemi, J. V., Kupiainen, K., Kulmala, M., and Vehkamäki, H.: Fatty acids on continental sulfate aerosol particles, J. Geophys. Res., 110, D06207, doi:10.1029/2004JD005400, 2005.
Tunved, P., Nilsson, E. D., Hansson, H. C., Strom, J., Kulmala, M., Aalto, P., and Viisanen, Y.: Aerosol characteristics of air masses in northern Europe: Influences of location, transport, sinks, and sources, J. Geophys. Res., 110, D07201 doi:10.1029/2004JD005085, 2005.
Vallius, M., Lanki, T., Tiittanen, P., Koistinen, K., Ruuskanen, J., and Pekkanen, J.: Source apportionment of urban ambient $PM_{2.5}$ in two successive measurement campaigns in Helsinki, Finland. Atmos. Environ., 37, 615–623, 2003.
van Poppel, L. H., Friedrich, H., Spinsby, J., Chung, S. H., Seinfeld, J. H., and Buseck, P. R.: Electron tomography of nanoparticle clusters: Implications for atmospheric lifetimes and radiative forcing of soot, Geophys. Res. Lett., 32, L24811, doi:10.1029/2005GL024461, 2005.
WHO: Health aspects of air pollution with particulate matter, ozone and nitrogen dioxide. Working group report, 13–15 January 2003, World Health Organization, Bonn, 2003.
Wittmaack, K., Wehnes, H., Heinzmann, U., and Agerer, R.: An overview on bioaerosols viewed by scanning electron microscopy, Sci. Total Environ., 346, 244–255, 2005.
Zhang, Q., Canagaratna, M. R., Jayne, J. T., Worsnop, D. R., and Jimenez, J. L.: Time- and size-resolved chemical composition of submicron particles in Pittsburgh: Implications for aerosol sources and processes, J. Geophys. Res., 110, D07S09, doi:10.1029/2004JD004649, 2005.
Zuberi, B., Johnson, K. S., Aleks, G. K., Molina, L. T., and Laskin, A.: Hydrophilic properties of

aged soot, Geophys. Res. Lett., 32, L01807, doi:10.1029/2004GL021496, 2005.

Table 1. Arithmetic means of meteorological variables, $PM_{1.6}$ mass concentrations and gas concentrations during sampling periods for TEM/EDX analysis (maximums shown in bold).

Sample number	Date	Time UTC	T (^oC)	RH (%)	Wind speed (m s^{-1})	Wind direction (degree)	$PM_{1.6}$ ($\mu g\ m^{-3}$)	O_3 (ppb)	CO (ppm)	SO_2 (ppb)	NO_2 (ppb)	NO (ppb)
6	06 May 2004	12:33–14:33	23	29	2.8	151	16.2	62	160	**0.63**	–	–
7	07 May 2004	10:44–11:44	22	31	4.2	92	**18.9**	**65**	**169**	0.50	**2.1**	0.03
10	10 May 2004	07:53–09:53	8	82	4.1	35	5.1	27	148	0.06	**2.1**	**0.22**
17	17 May 2004	06:58–10:58	9	36	3.6	278	2.6	40	135	0.12	0.9	0.07
20	20 May 2004	08:56–13:26	9	42	5.7	299	2.0	37	128	0.06	0.6	0.04
22	22 May 2004	08:49–14:49	9	46	5.9	331	2.4	39	129	0.07	0.7	0.04

ACPD
6, 6753–6799, 2006

Table 2. Mass concentrations of total particle mass, ions, OC and EC in $PM_{1.3}$ and $PM_{1.3-10}$ size fractions during different sampling periods, and their relative proportions (%) of total particle mass. Maximum values of each component in both size fractions are shown in bold.

	Pollution episode	Intermediate period	Clean marine period			Pollution episode	Intermediate period	Clean marine period		
Start date	07 May	09 May	16 May	20 May	22 May	07 May	09 May	16 May	20 May	22 May
End date	09 May	11 May	18 May	22 May	24 May	09 May	11 May	18 May	22 May	24 May
	($ng\,m^{-3}$)	($ng\,m^{-3}$)	($ng\,m^{-3}$)	($ng\,m^{-3}$)	($ng\,m^{-3}$)	(%)	(%)	(%)	(%)	(%)
$PM_{1.3}$										
Mass	**16 000**	6300	2400	1500	1100					
NO_3^-	**42**	14	24	24	6.6	0.26	0.23	1.0	**1.6**	0.58
SO_4^{2-}	**4600**	1900	750	430	340	28.3	30.7	**31.3**	28.1	29.5
Cl^-	1.9	0.7	0.6	**4.8**	0.1	0.01	0.01	0.02	**0.32**	0.01
MSA	21	22	**110**	96	33	0.13	0.34	4.55	**6.3**	2.91
Oxalate	**120**	43	11	9.9	7	**0.77**	0.69	0.44	0.65	0.61
Succinate	**66**	33	10	5.5	2.6	0.41	**0.52**	0.42	0.36	0.23
Malonate	**22**	13	3.3	1.5	0.6	0.13	**0.21**	0.14	0.1	0.05
Na^+	**25**	21	22	19	6.6	0.16	0.34	0.93	**1.27**	0.58
NH^{4+}	**1600**	670	270	160	120	10.1	10.6	**11.4**	10.3	10.4
K^+	**150**	42	18	8.8	4	**0.9**	0.66	0.74	0.57	0.35
Mg^{2+}	2	2.2	2.2	3	0.9	0.01	0.04	0.09	**0.2**	0.08
Ca^{2+}	**8.8**	4.2	4.2	1.5	0.1	0.05	0.07	**0.17**	0.1	0.01
$\sum MA$[a]	**15**	8.3	1.7	3.4	1.1	0.09	0.13	0.07	**0.23**	0.1
EC	**520**	160	100	76	100	3.25	2.49	4.26	4.99	**8.74**
OC[b]	**5100**	2100	730	460	400	31.4	33.4	30.1	30.3	**34.5**
Unidentified[c]	**4100**	1400	480	340	170	**25.5**	21.5	20.0	22.4	15.3
$PM_{1.3-10}$										
Mass	**4200**	1900	1500	740	690					
NO_3^-	**370**	110	110	41	15	**8.72**	6.03	7.36	5.58	2.2
SO_4^{2-}	**330**	190	57	46	31	7.84	**10**	3.74	6.21	4.51
Cl^-	3.5	19	37	**68**	14	0.08	1.03	2.39	**9.17**	2.01
MSA	0.1	1.7	4.3	**5.1**	1.9	0	0.09	0.28	**0.69**	0.28
Oxalate	**17**	9.2	5.2	8.1	5.9	0.41	0.49	0.34	**1.09**	0.86
Succinate	7.2	4.8	0	**8.3**	5.8	0.17	0.25	0	**1.12**	0.84
Malonate	**16.7**	4.9	1.5	0.5	0	**0.40**	0.26	0.09	0.06	0
Na^+	16	33	**54**	**54**	14	0.39	1.74	3.5	**7.23**	1.98
NH^{4+}	**78**	37	12	8.2	8.9	1.84	**1.95**	0.79	1.1	1.29
K^+	**42**	9.8	2.7	3.1	3.6	**1.01**	0.52	0.18	0.42	0.52
Mg^{2+}	**13**	8	8.9	8.8	2.6	0.31	0.43	0.58	**1.18**	0.38
Ca^{2+}	**170**	61	25	7	4.2	**4.06**	3.27	1.61	0.94	0.61
$\sum MA$[a]	**0.5**	–	–	–	–	0.01	–	–	–	–
EC	90	84	69	72	**100**	2.15	4.46	4.53	9.65	**14.5**
OC[b]	**1900**	1600	1100	430	360	45.5	**83.8**	70.2	57.8	51.8
Unidentified[c]	**1200**	−250	79	5	140	**28.1**	−13.3	5.1	0.7	20.2

[a] $\sum MA$ = levoglucosan + galactosan + mannosan.

[b] OC = organic carbon + carbonate carbon.

[c] Unidentified = particle mass − (NO_3^- + SO_4^{2-} + Cl^- + Na^+ + NH^{4+} + K^+ + Mg^{2+} + Ca^{2+} + EC + OC). The one negative value probably results from an inaccuracy in OC analysis due to low particle concentrations.

ACPD
6, 6753–6799, 2006

EGU

Table 3. Classification criteria for different particle groups.

Particle group	Elemental characteristics *	Typical morphology/internal structure and beam sensitivity
Tar balls	Abundant C with minor S, often minor K	Individual particles with circular shape
Soot	Abundant C, often minor S, K and/or Si	Fractal-like agglomerates of circular particles
Soot/sulphate mixture	Abundant C and/or S, often minor K and/or Si	Soot on surface or inside circular particles, beam damage
Carbon/sulphate mixture with dark inclusion(s) **	Abundant C with variable S, often minor K	Mostly circular shape, contains dark inclusion(s), beam damage
Ammonium sulphates with/without carbon and dark inclusion(s)	Abundant S with variable C, often minor K	Mostly circular shape, seldom minor dark inclusion(s), beam damage
K-rich with S and/or C	Abundant K with S and/or C	Mostly circular shape, sometimes dark inclusions, often beam damage
Ca/Mg carbonate, sulphates and/or nitrate	Abundant Ca with C and/or S, sometimes with abundant Mg and/or minor Si	Mostly circular shape, sometimes angular
Silicates	Abundant Si, usually with Al, variable minor Fe, Ca, K, Mg, Na, Ti,and/or S	Irregular soil particles or circular fly ashes
Metal oxides/hydroxides	Abundant Mn, Fe, Zn and/or Pb	Irregular angular or circular particles
Sea salt and other Na-rich particles	Abundant Na, variable Cl, S, Mg, K, Ca	Variable morphology; angular, circular, sponge-like porous
Biological particles	Abundant C, usually minor K and/or P	Variable morphology
C-rich fragments	Abundant C	Angular shape, often thin

*Oxygen was present in practically all particles, and therefore, it is not shown in the element lists.

**X-ray counts of carbon >35% from the total net counts of elements with $6 \geq Z \geq 82 = 100\%$.

ACPD
6, 6753–6799, 2006

Table 4. Relative abundances (%) of particles in different particle groups in three size fractions during the six sampling periods in May 2004. *

Size fraction	0.2 μm <Dp< 1 μm						1 μm <Dp< 3.3 μm						3.3 μm<Dp<11 μm					
	Pollution episode		Intermediate period	Clean marine period			Pollution episode		Intermediate period	Clean marine period			Pollution episode		Intermediate period	Clean marine period		
Sample number (= date)	6	7	10	17	20	22	6	7	10	17	20	22	6	7	10	17	20	22
Tar balls	1	2	0	0	0	0	**4**	**4**	2	0	0	0	0	0	0	0	0	0
Soot	7	3	**12**	0	3	6	0	0	2	0	0	0	11	5	0	0	0	0
Soot/sulphate mixture	13	4	**22**	12	3	2	0	0	0	0	0	0	0	0	0	0	0	0
Carbon/sulphate mixture with dark inclusion(s)	7	**10**	4	8	4	5	0	0	0	0	0	1	0	0	0	0	0	0
Ammonium sulphates with/without carbon and dark inclusion(s)	59	72	54	66	**89**	86	9	14	5	6	2	14	0	0	0	5	0	0
K-rich with S and/or C	5	1	3	**9**	1	0	0	0	0	0	0	0	0	0	0	0	0	0
Ca/Mg carbonates, sulphates and/or nitrates	1(1)	0	0	0	0	0	**48**(22)	39(27)	3(3)	10(6)	2(2)	1(1)	26(21)	38(29)	6(6)	0	5(5)	0
Silicates	4(1)	4(2)	0	3	0	0	22(1)	26(7)	14(2)	17	2	5	32	33	0	**53**	5	6
Metal oxides/hydroxides	1	4(2)	0	1	0	1	4(1)	9(1)	0	0	0	3(1)	5	5(5)	**11**(6)	0	0	3
Sea salt and other Na-rich particles	1	0	3	1	0	0	9	4	71	67	**89**	73	5	0	11	21	25	0
Biological particles	0	0	0	0	0	0	0	0	2	0	2	0	21	14	50	0	55	**81**
C-rich fragments	1	1	2	0	0	1	5	4	2	0	5	3	0	5	**22**	21	10	10
Number of analysed particles (n)	136	103	104	100	102	103	85	74	63	63	64	73	19	21	18	19	20	31

*Maximum value of each particle group is shown with bold numbers. The values in parentheses show the abundances of spherical/rounded particles.

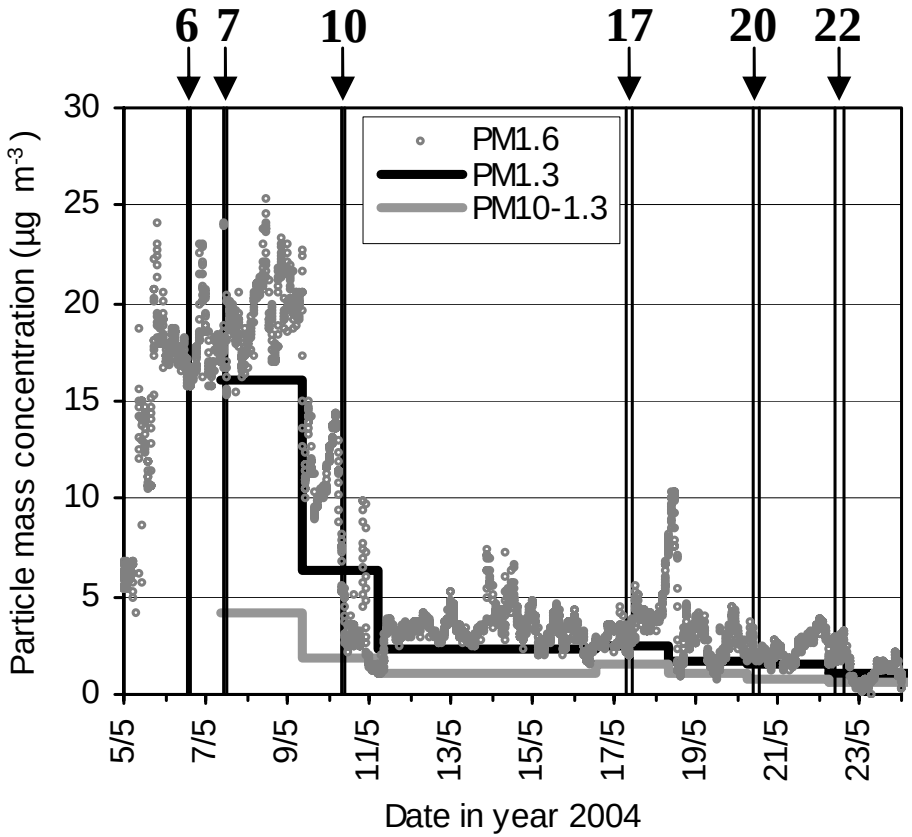

Fig. 1. Particle mass concentrations ($PM_{1.6}$ measured with ELPI, and $PM_{1.3}$ and $PM_{1.3-10}$ with VI) in Hyytiälä in May 2004. The six sampling periods with the Battelle impactor for TEM/EDX analysis are marked with vertical lines and arrows (sample numbers above).

ACPD
6, 6753–6799, 2006

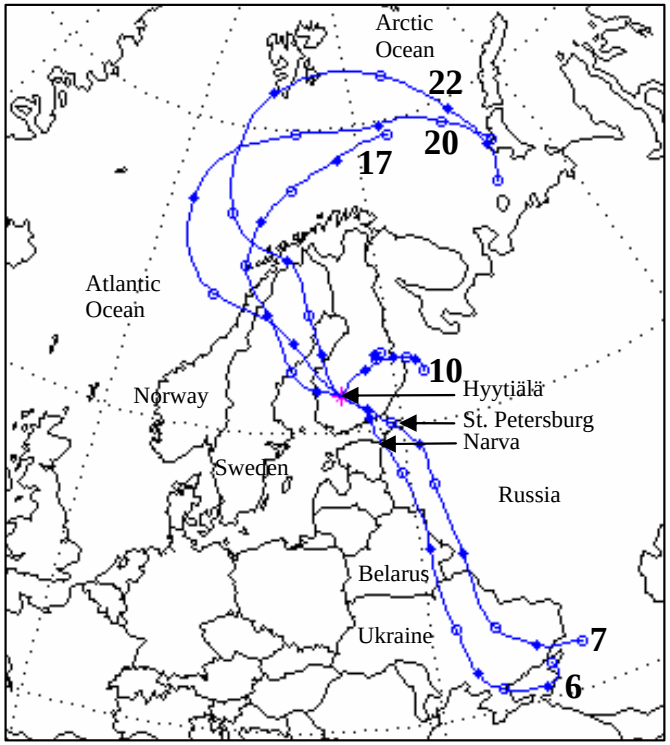

Fig. 2. Backward air mass trajectories arriving at 250 m level to Hyytiälä during the six sampling periods in May 2004. Date numbers (=sample numbers) of each trajectory are shown, and symbols represent 12-h intervals (total time 96 h).

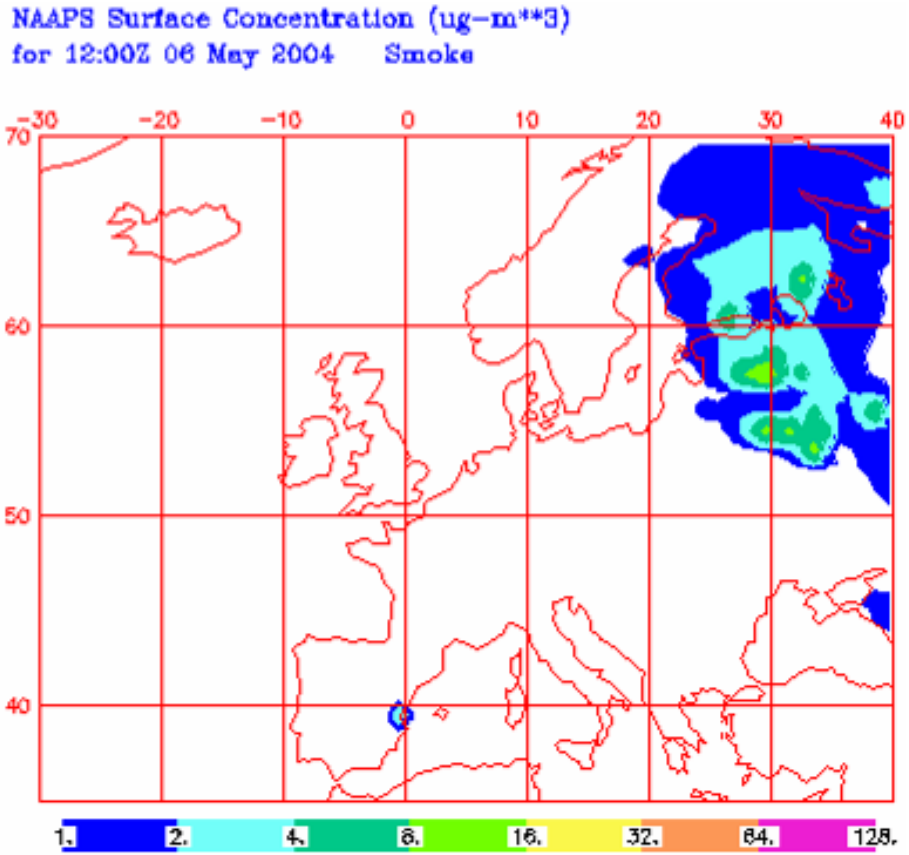

Fig. 3. NAAPS model results showing surface smoke concentrations in Europe at 12:00 (UTC) on 6 May 2004 (Naval Research Laboratory, Monterey, CA, USA, website at http://www.nrlmry.navy.mil/aerosol/).

ACPD
6, 6753–6799, 2006

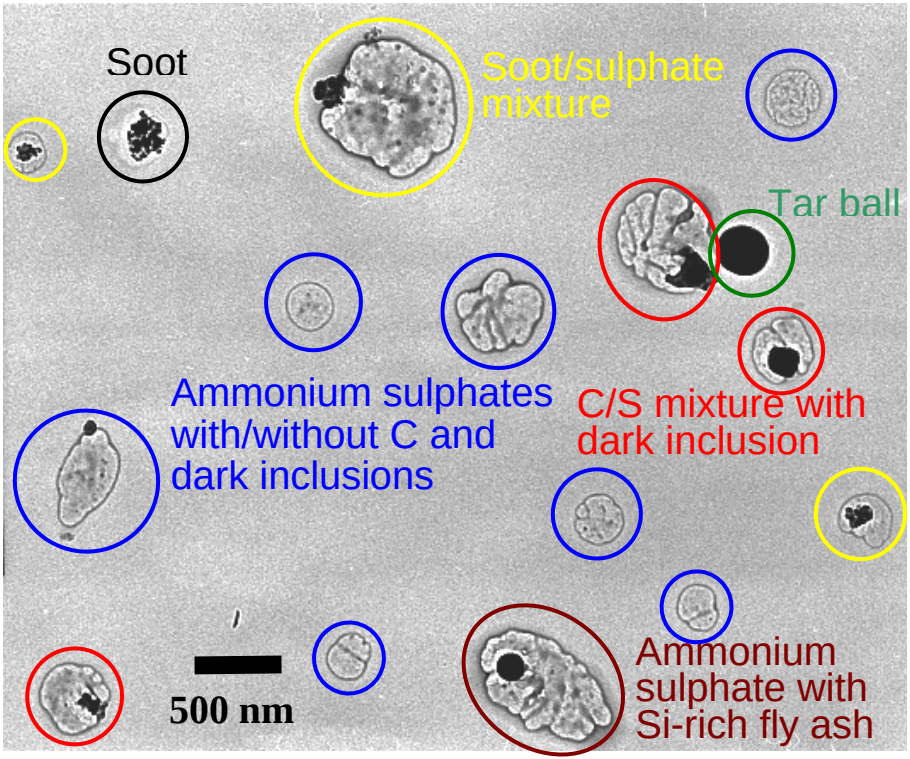

Fig. 4. TEM image of different particle types from $PM_{0.2-1}$ sample 7 collected during the pollution episode.

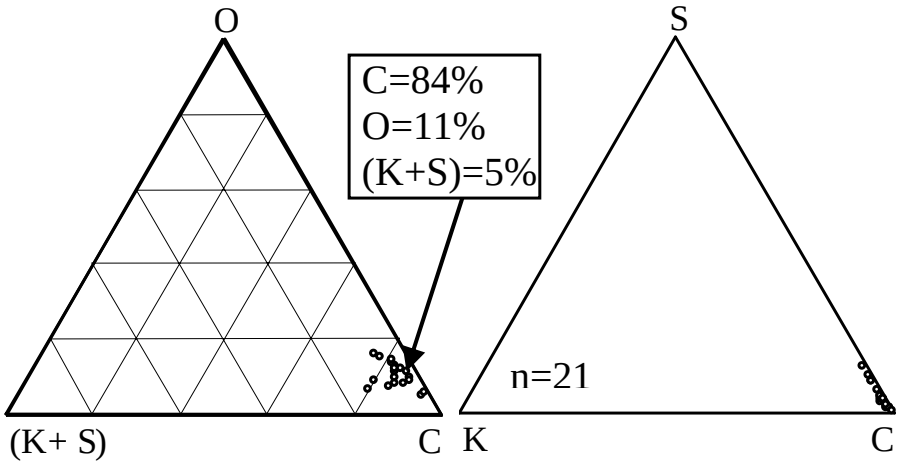

Fig. 5. Ternary diagrams of C-O-(K+S) and C-S-K ratios for tar balls collected during the pollution episode ($PM_{0.2-1}$ and $PM_{1-3.3}$ samples 6–7). The X-ray count sum of the selected elements is normalized to 100%, and an example of the elemental ratios is shown in the box.

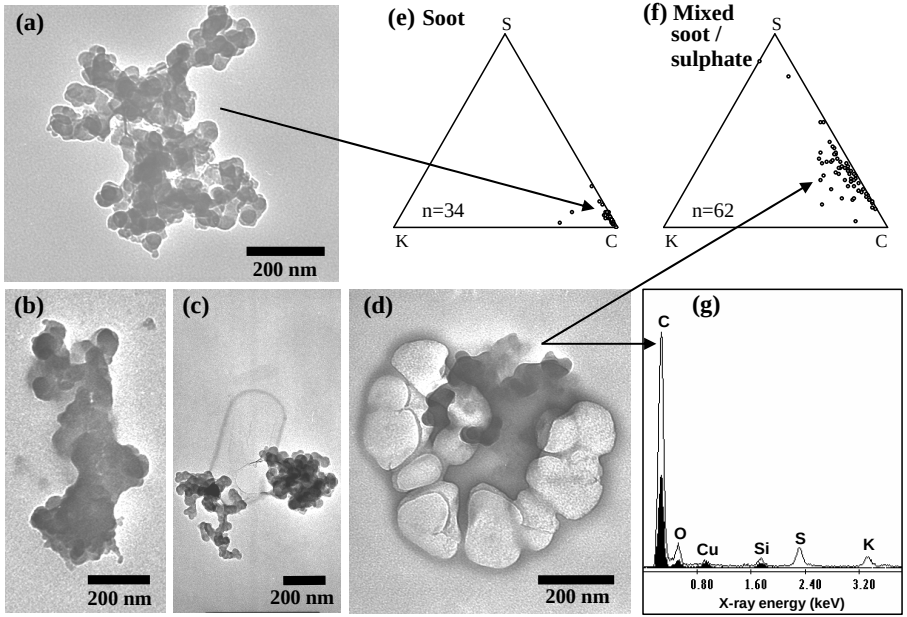

Fig. 6. TEM images of **(a)** soot, **(b)** mixed soot/sulphate particle, **(c–d)** mixed soot/sulphate particles after intentional strong beam exposure, **(e–f)** C-S-K ternary diagrams for these particle types from all $PM_{0.2-1}$ samples, and **(g)** X-ray spectrum for the soot/sulphate particle (background spectrum from TEM grid substrate is depicted in black).

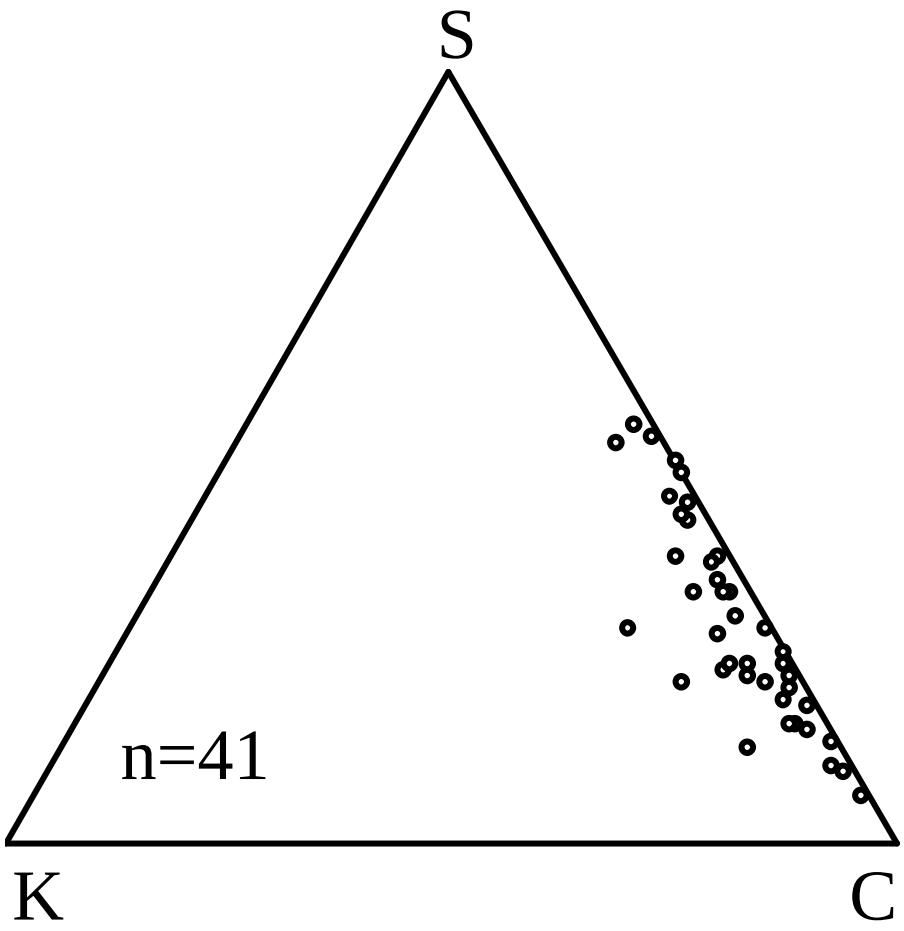

Fig. 7. Ternary diagram of C-S-K ratios for particles in "carbon/sulphate mixture with dark inclusion(s)" group from all $PM_{0.2-1}$ samples.

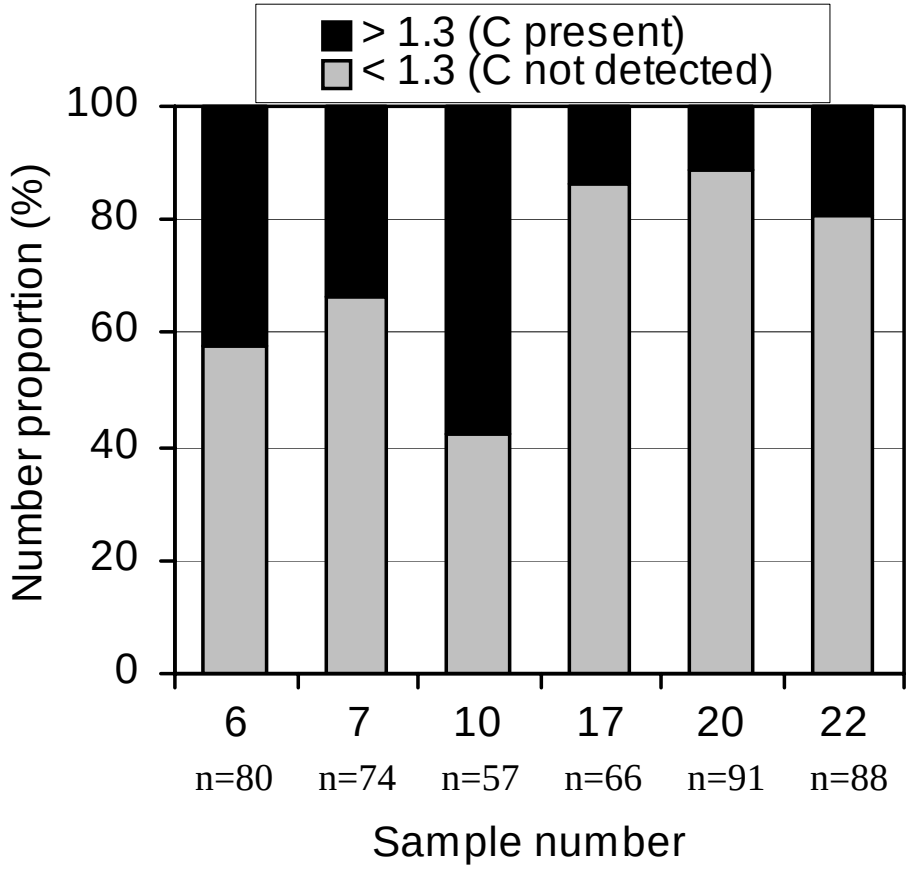

Fig. 8. Relative proportion of ammonium sulphate particles with detectable carbon (with total C peak to background C peak ratio >1.3 as indicator) and without detectable carbon (the same ratio <1.3) from $PM_{0.2-1}$ samples.

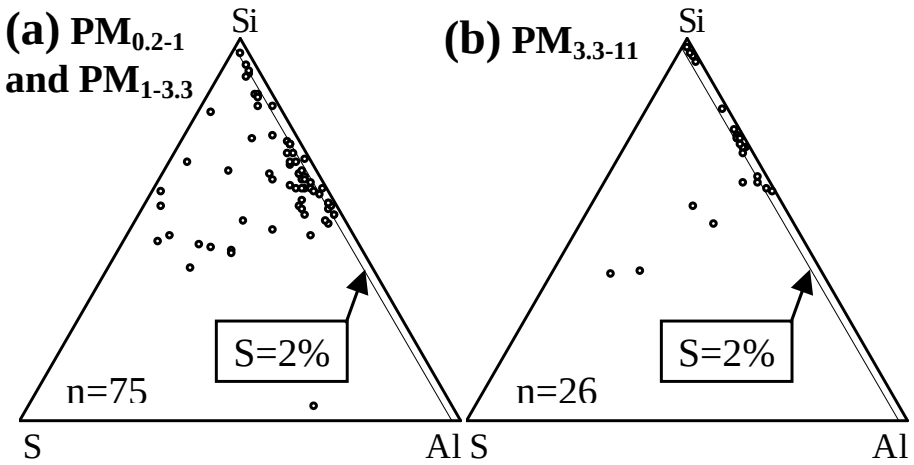

Fig. 9. Ternary diagrams of Al-Si-S ratios for silicates from all **(a)** $PM_{0.2-1}$ and $PM_{1-3.3}$ samples and **(b)** $PM_{3.3-11}$ samples.

ACPD
6, 6753–6799, 2006

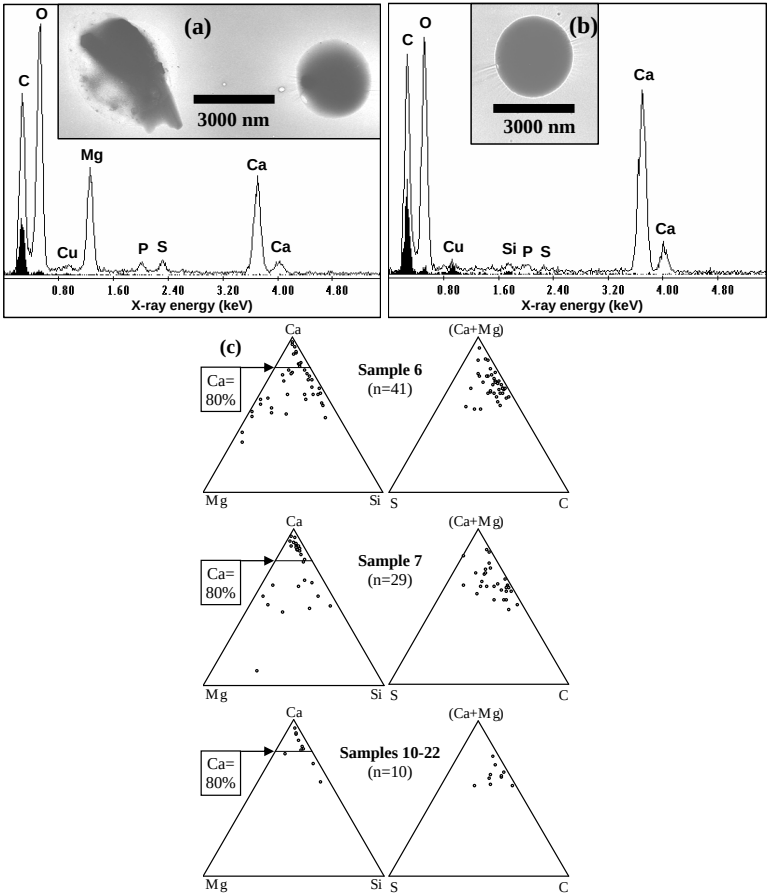

Fig. 10. TEM images of Ca-rich particles **(a)** with abundant Mg and **(b)** without Mg together with their X-ray spectra (from the spherical particles), and **(c)** ternary diagrams of Si-Ca-Mg and C-(Ca+Mg)-S ratios for Ca-rich particles from selected $PM_{1-3.3}$ samples.

ACPD
6, 6753–6799, 2006

EGU

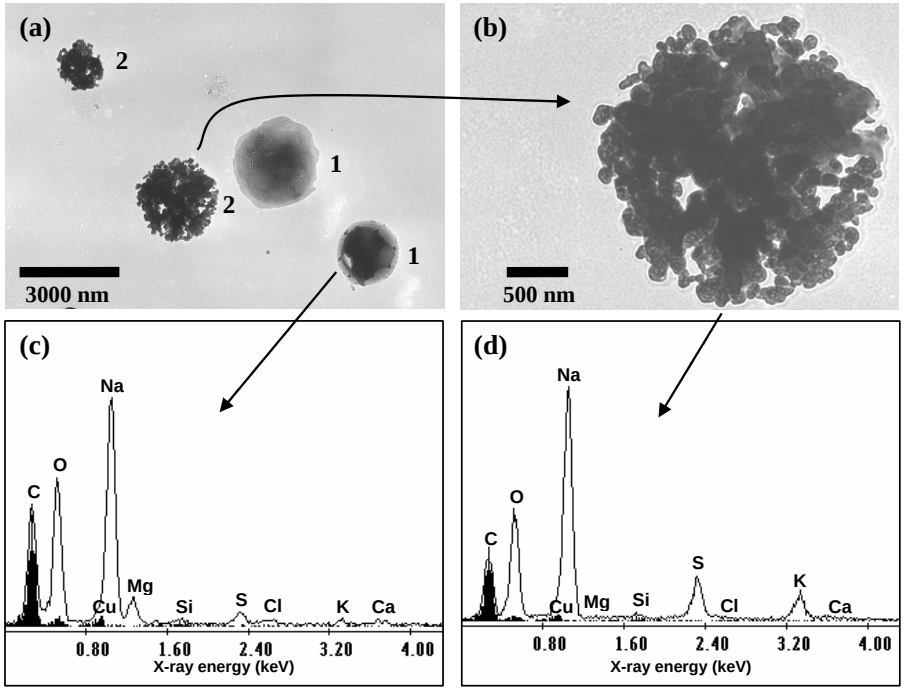

Fig. 11. TEM images of **(a1)** sea salt particles with strong Cl depletion and **(a2)** and **(b)** porous Na-S-K-O-rich particles. The X-ray spectra **(c)** and **(d)** show that porous particle did not contain Mg and Ca and that the proportion of K was high compared to elemental ratios in sea salt (background spectra from TEM grid substrate are depicted with black colour).

ACPD
6, 6753–6799, 2006

EGU

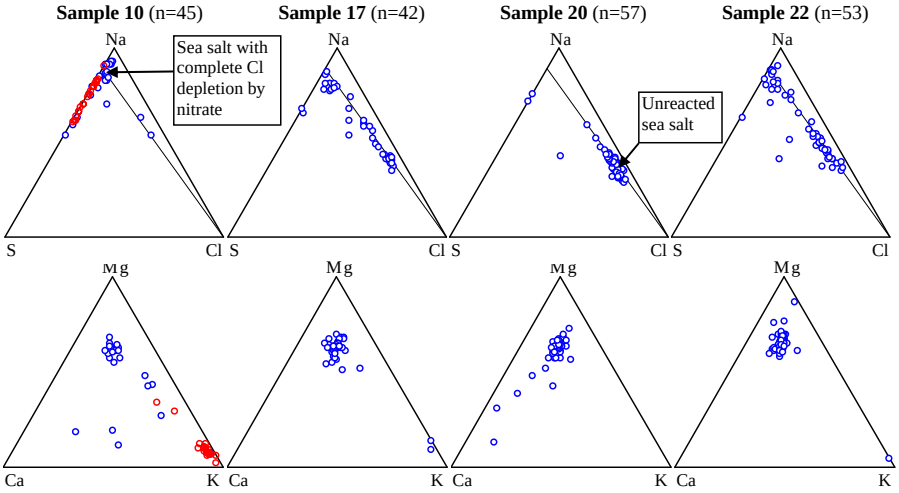

Fig. 12. Ternary diagrams of Cl-Na-S (top row) and K-Mg-Ca (bottom row) ratios for all sea salt particles (blue symbols) and porous Na-S-K-O-rich particles (red symbols) in selected $PM_{1-3.3}$ samples. The line in Cl-Na-S diagrams depicts the constant S/Na ratio, which is the same as in unreacted sea salt particles. When symbols of sea salt particles are located clearly below that line, they indicate substitution of Cl by S-containing anions such as sulphate or MSA.

ACPD
6, 6753–6799, 2006

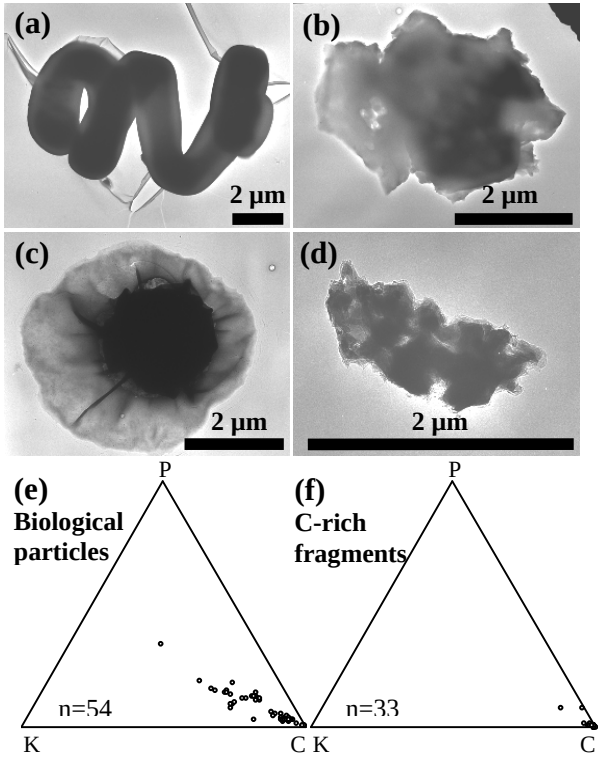

Fig. 13. TEM images of particles classified as **(a, c)** biological particles and **(b, d)** C-rich fragments, as well as **(e, f)** ternary diagrams of C-P-K ratios for these particles from all samples.

ACPD
6, 6753–6799, 2006